Nondestructive Testing for Multi-Layer Metal-Metal Bonded Structure by Using Inductive Lock-In Thermograhy

Yuyu Zhu, Bin Gao, *Senior Member, IEEE*, Gui Yun Tian, *Senior Member, IEEE*, Wai Lok Woo, *Senior Member, IEEE*, Guangping Tang, Chaoming Sun, and Jianwen Li

***Abstract*— Multilayer materials with metal–metal bonded structure have been widely applied in aviation, aerospace and nuclear industrial fields. The presence of inner defects such as debonding, air gaps leads to significant degradation of the load capacity and mechanical behaviors. Due to their complex structure, debonding detection in metal–metal structure inherently remains challenge. This paper proposes a feasibility study of non-destructive inspection of debonding defect in lead-steel sample by using inductive lock-in thermography (ILT). The detectability validation is carried out based on experimental studies. Theoretical analysis, excitation source and system design as well as various influence parameters of ILT are discussed and optimized. Fourier-transform based post-processing has been investigated to analyze both magnitude and phase images for defects identification. The obtained results have been promising validated and it indicated the ability to improve the signal-to-noise ratio. The comparative experiment using different methods (ILT, ECPT, and OLT) has been carried out. The results have revealed that the ILT has advantages and could be served as a strong candidate for practical adoption in debonding defect inspection in metal–metal bonded sample.**

***Index Terms*— Multi-layer metal-metal bonding structure, non-destructive technique, inductive lock-in thermography, detectability sensitivity.**

I. Introduction

An ADHESIVE is defined as a polymeric substance with viscoelastic behavior which can hold adherends together by surface attachment to produce a joint with a high shear strength. Adhesive bonding is a popular method of joining metallic and non-metallic structures offering essential advantages, such as higher joint stiffness and superior fatigue performance. Those adhesive bonded structures including metal-metal, metal-plastic, metal-composite, composite-composite, plastic-plastic, metal-ceramic, are being widely applied in aviation, aerospace, rail vehicles and nuclear industrial fields [1]. However, these bonded structures are prone to defects including poor adhesion, less cohesive strength, voids, disbonds and porosity during the manufacturing process and in service phase which will lead to degradation of the materials performance and reduction of life [2]. Thus, in order to guarantee the quality, bonded structure is required to be monitored by effective non-destructive technique (NDT) such as X-ray, infrared thermography and various ultrasound methods.

In [3] and [4], composite adhesive lap joints produced from a bi-directional woven E-glass fibres and polypropylene including the effects of layer orientation, lap joint length and water immersion on the fatigue behavior were studied. In [5]–[8], several NDT methods including induction thermography, optical thermography, vibrothermography and ultrasound excited thermography were proposed to inspect and evaluate various defects of the composite-composite structure materials such as carbon-fibre-reinforced polymer (CFRP).

In addition, metal-nonmetal bonding structure has attracted research attention. In [9] and [10], the behavior of FRP-steel bonded interfaces was studied and the fatigue behavior, bond and force transfer mechanisms were discussed. In [11]–[14], the honeycomb sandwich material is investigated which has a typical metal-nonmetal bonding structure. It usually consists of three main parts: two thin, stiff skin faces with high density and a thick core material with low density. Composite laminates or metallic materials such as aluminum alloy or steel can be used as skin faces. In NDT, Ultrasonic C-scan, X-rays, active thermograhphy are used to detect various defects of the bonded material such as debonding, water deposit, scratches, cracks, air holes, and damages of core.

As discussed above, research on multi-layered nonmetal-nonmetal and metal-nonmetal adhesive bonded structure has already been studied and tends to be ripe. Nevertheless, those of multi-layered metal-metal adhesive structure are rarely investigated. Lead-steel bonded structure is generally applied in the nuclear industry due to its special characteristics such as anti-nuclear radiation, high strength and anti-fatigue. However, defects such as debonds, porosity, air gaps, etc., appears during manufacturing process and in-servers stage. These defects will affect the integrity of the bonded structure and lead to degradation performance. Thus, it is highly required to

Manuscript received July 15, 2017; accepted August 11, 2017. Date of publication August 18, 2017; date of current version September 25, 2017. This work was supported in part by NSAF under Grant U1430115 and in part by the National Natural Science Foundation of China under Grant 51377015, Grant 61401071, and Grant 61527803. The associate editor coordinating the review of this paper and approving it for publication was Dr. Chao Tan. *(Corresponding author: Bin Gao.)*

Y. Zhu is with the University of Electronic Science and Technology of China, Chengdu 611731, China (e-mail: zhuyuyu_008@163.com).

B. Gao is with the School of Automation Engineering, University of Electronic Science and Technology of China, Chengdu 611731, China (e-mail: bin_gao@uestc.edu.cn; bin.gao@ncl.ac.uk).

G. Y. Tian and W. L. Woo are with the University of Newcastle, Newcastle NE1 7RU, U.K. (e-mail: g.y.tian@ncl.ac.uk; lok.woo@ncl.ac.uk).

G. Tang is with the China Academy of Engineer Physics, Mianyang 621900, China.

C. Sun and J. Li are with the Institute of Machinery Manufacturing Technology, China Academy of Engineering Physics, Mianyang 621900, China.

Digital Object Identifier 10.1109/JSEN.2017.2741581

adopt suitable NDT technique to assurance the product quality. Conventional detection method such as C-scan and X-ray are limited due to a long time-consuming, unsafe, and require of bulky instruments, which makes it unsuitable to be directly applied to lead-steel bonded material. Ultrasonic testing (UT) based on the propagation of ultrasonic waves in the object has good detectability for inner defects. However, common UT method is not convenient for detecting lead-steel sample because that it requires couplant. Compared with the conventional detection method, the active infrared thermography is a potential technique which can be applied to detect and evaluate defect of lead-steel bonded structure.

Active infrared thermography utilizes an external excitation source of energy to induce a temperature difference between defective and non-defective areas in the specimen under examination. Due to different external excitation source, active thermography can be divided into inductive thermography, optical thermography and vibro-thermograph among others [15]. The debonding of lead-steel bonded structure can be considered as inner defect of metal. Inductive thermography (IT) system which combines two techniques: Eddy Current (EC) and thermography [13] has the potential with an increasing span of applications [14]. Comparing with other thermography NDT&E systems, the heat of IT is not limited to the sample surface, rather it can reach a certain depth, which governed by the skin depth of eddy current. Eddy current pulse thermography (ECPT) and inductive lock-in thermography (ILT) are most commonly two types of inductive thermography. Compare with ECPT, ILT has longer thermal diffusion length whereas deeper defect can be inspected with higher signal-to-noise ratios (SNRs) [16]. Thus, it has potential to be a suitable candidate for inspecting debonding defects for lead-steel sample.

ILT can be used for conductive material, which combines the advantages of lock-in mode excitation and inductive thermography. G.Riegert et.al. proposed the ILT method for crack detection in metals, delamination damage assessment of C/C-SiC and impact damage assessment of CFRP samples [17], [18]. Johannes Bohm et.al. used ILT method for defects inspection of solder joints on SMD packages and for electrics packages and modules [19], [20]. Previous work has focused on the application of ILT technology whereas the physics mechanism and the design of excitation source are rarely investigated. This paper proposes the feasibility study for debonding defect detection of lead-steel bonded structure which utilizes eddy current lock-in thermography. The contributions of the work lie in the development of the physics mechanism that underlies the ILT system with lead-steel structrure and the design of the excitation source according to the inductive lock-in thermography. Due to the performed Fourier analysis of the temperature image sequence, the signal-to-noise ratio in the magnitude and phase images is discussed. Experimental tests on real experiments and comparative studies have been conducted to show the validity of the proposed method.

The paper is organized as follows: Section II discusses the physics model of ILT mechanism and Fourier analysis. Section III describes the experimental setup. Sections IV and V present the experiment results and discussion. Finally, Section VI concludes the work.

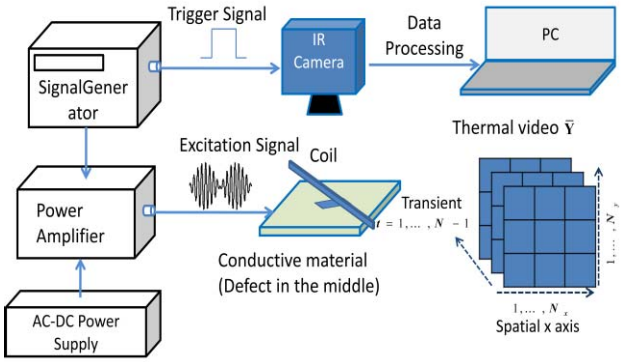

Fig. 1. Inductive lock-in thermography diagram.

II. Methodology

A. Derivation of Inductive Lock in Thermography

Fig. 1 shows the diagram of the inductive lock-in thermography system. An induction coil is driven by amplitude-modulated current and the induced current in the conductive material generates time-varying heat sources. The heat will diffuse in time until it reaches an equilibrium state in the material. The distribution of temperature on the surface of material is recorded by infrared (IR) camera and the sequence of infrared images are transmitted to a computer for signal process. Defects such as cracks, debonds, delamination results in inhomogeneity inside the material which alters the eddy current distribution and the heat diffusion.

The governing equation describing the EM field in ILT system can be deduced from Maxwell's equations, for time-varying fields [21], namely

$$\nabla \times \frac{1}{\mu}\nabla \times \mathbf{A} + \sigma \frac{\partial \mathbf{A}}{\partial t} + \varepsilon \frac{\partial^2 \mathbf{A}}{\partial} t^2 = -\sigma \nabla \mathbf{A} - \varepsilon \nabla \frac{\partial V}{\partial t} \quad (1)$$

where $\mathbf{A}$ is the magnetic vector potential, V is the electric scalar potential. μ is magnetic permeability, σ is the electrical conductivity and ε is permittivity of the medium. As excitation frequency of ILT is typically chosen from dozens to several hundred kHz, whereas electric displacement vector D can be ignored in the metallic material [22]. Thus, as regions with homogeneous and uniform magnetic material properties, (1) can be written as:

$$\frac{1}{\mu}\nabla^2 \mathbf{A} - \sigma \frac{\partial \mathbf{A}}{\partial t} = -\mathbf{J} \quad (2)$$

where $\mathbf{J} = -\sigma \nabla V$ is the given electric current density. Eq.(2) is a second-order differential equation which can be solved after setting the boundary conditions using the FEM approach [23]. Thus, the value of magnetic vector potential $\mathbf{A}$ can be obtained. Subsequently, the electric field intensity vector $\mathbf{E}$ and the induced current density $\mathbf{J_e}$ can be calculated by the Eq.(3) and Eq.(4), namely

$$\mathbf{E} = -\frac{\partial \mathbf{A}}{\partial t} \quad (3)$$

$$\mathbf{J}_e = \sigma \mathbf{E} \quad (4)$$

TABLE I
δ AND μ_{th} OF STEEL AND LEAD WITH DIFFERENT f_{ind} AND f_{lock}

	Skin depth δ in mm		Thermal diffusion length μ_{th} in mm			Thermal conductivity k W/mK	Electrical conductivity σ S/m	Specific heat c_p J/kg · K	Density ρ kg/m^3	Relative permeability μ_r	thermal diffusity α m^2/s
f_{ind} /f_{lock}	47.5 kHz	100 kHz	0.1 Hz	0.5 Hz	10 Hz						
Steel	0.1	0.07	6.5	2.9	0.6	46	1.0E-08	440	7900	500	132
Lead	1.05	0.72	8.8	3.9	0.9	35.3	4.8E-08	129	11340	1	241

In a semi-infinite plane with sinusoidal excitation, the amplitude of induced current density $\mathbf{J_e}$ decays exponentially towards the interior of the conducting media, falling to $1/e$ of the value at the surface in a distance called the eddy current penetration depth ("skin depth"):δ

$$\delta = \frac{1}{\sqrt{\pi \mu \sigma f_{ind}}} \tag{5}$$

where f_{ind} is induction frequency ("excitation frequency").

The induced current density $\mathbf{J}_\mathrm{e}$ generates resistive heat Q which is proportional to the square of its magnitude. According to inductive heat conduction equation [19], [24], thermal diffusion length μ_{th} can be expressed as:

$$\mu_{th} = \sqrt{\frac{\alpha}{\pi \cdot f_{lock}}} = \sqrt{\frac{k}{\pi \cdot f_{lock} \cdot \rho c_p}} \tag{6}$$

where α is thermal diffusity (m^2/s),k is the thermal conductivity (W/mK),ρ is the density (kg/m^3), c_p is specific heat (J/kg · K), f_{lock} is the lock-in frequency.

The probing depth of the defects depends on two factors: eddy current penetration depth δ and penetration depth of the thermal wave p. Here p is defined as the depth of the defects from the heat source. The value of p equals μ_{th} for amplitude images, $1.5\mu_{th}$ to $2\mu_{th}$ for phase images [25], [26]. For the metallic material, due to the higher induction frequency f_{ind}, the eddy current penetration depth δ is small. In Table.I, the penetration depth of the eddy current δ of the steel and lead is only 0.07 mm and 0.72 mm, respectively under $\mathrm{f_{ind}}$= 100kHz. Conversely, the penetration depth of the thermal wave p of the steel and lead can reach more than 9.7 mm and 13.2 mm, respectively under lock-in frequency f_{lock}= 0.1 Hz. Thus, p is a dominant factor for inspection of debonding defect of the lead-steel sample.

Compare to ECPT and ILT system, they have same eddy current penetration depth under the same excitation frequency. However, they have different thermal wave penetration depth. In ECPT, the thermal wave penetration depth z relates to propagation time t, the relationship is described by Eq.(7) [27]. In order to detect deeper defects, propagation time t should be prolonged. This procedure increases possibility to damage the sample due to strong excitation current (usually hundreds amperes). In addition, propagation time including both the heat time and cool time whereas it should be selected and optimized manually to obtain better results. This brings subjective issues.

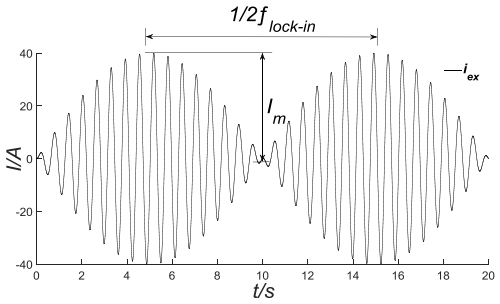

Fig. 2. Profile of the excitation current.

$$z \sim \sqrt{\alpha t} \tag{7}$$

In ILT system, supposed that the properties of the material and the depth range of the defect are known, it is easy to obtain the suitable lock-in frequency by using (5) and (6). In addition, current excitation in ILT system is adjusted smaller than that of the ECPT system. This reduces the possibility of damage on the sample as well as avoiding manually selection of heating time in ECPT.

B. Fourier Analysis

The excitation current which drives the induction coil is formed by combining a low frequency sinusoidal signal with a high frequency signal through amplitude modulated mode. The excitation current i_{ex} can be expressed as (8) and its profile is shown in Figure 2.

$$i_{ex}(t) = I_m \cdot \sin\left(2\pi f_{lock} t\right) \cdot \sin\left(2\pi f_{ind} t\right) \tag{8}$$

where I_m is the maximum of the amplitude, f_{lock} and f_{ind} are lock-in frequency and induction frequency, respectively.

Thus, the sample is heated periodically and the temperature on the surface of the sample varies periodically as well. Fig. 3 shows the diagram of temperature evolution of one point on the surface during the heating. Due to the frequency of temperature change is nearly equal to the lock-in frequency, the interference such as non-uniform heating, environmental reflections and surface emissivity variations can be suppressed extensively by using mathematical tool between the temporal and frequency domains - Fourier transform.

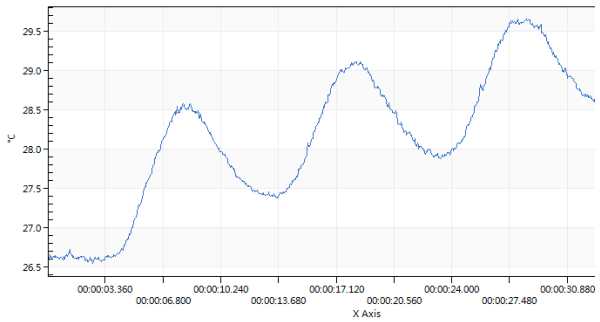

Fig. 3. The diagram of temperature evolution of one point on the surface during the heating.

For each pixel (i, j) in the thermal image, the temporal evolution of temperature $T(x)$ is extracted from the images sequence (where x is the index in the images sequence). Thus, Discrete Fourier transform is computed according to the well-known formula [27].

$$F(f)=\frac{1}{N}\sum_{x=0}^{N-1}T(x)\,exp\left[-\frac{j2\pi fx}{N}\right]=Re(f)+Im(f) \quad (9)$$

where $Re(f)$ and $Im(f)$ are the real and imaginary components of $F(f)$, respectively. N is the number of thermogram sequence. Finally, the magnitude and phase at specified frequency for all pixels can be extracted to obtain magnitude image and phase image by using Eq.(10).

$$\begin{aligned}|F(f)| &= \sqrt{\mathrm{Im}^2(f)+\mathrm{Re}^2(f)}\\ \emptyset(f) &= \arctan\frac{\mathrm{Im}(f)}{\mathrm{Re}(f)}\end{aligned} \quad (10)$$

The range of frequency spans from 0 to $1/\Delta x$ with the increment $\Delta f = 1/N\Delta x$,where Δx is the time interval between images, and $1/\Delta x$ is the sampling rate. In order to obtain the magnitude and phase image at lock-in frequency or some interest frequency, sample rate of the infrared (IR) camera $1/\Delta x$ and the number of thermogram sequence N should be set. For example, if the sample rate is set 12.5Hz, N= 1024 and $f_{lock} = 0.1$Hz , then the index of magnitude and phase image$k \approx 8$ can be obtained by using (11)

$$k=\frac{f_{lock}\cdot N}{1/\Delta x} \quad (11)$$

It should be noted that at least one lock-in period is required to guarantee the accuracy of post signal process.

C. Excitation Source Design of ILT

In Fig.1, the ILT system mainly includes excitation source, coil, IR camera, data process. The performance of the excitation source have great influence on the effect of defects inspection. In this study, the designed excitation source was introduced which adopts linear amplifiers to achieve high quality power signal. Compare to adopt the switching circuit as the power amplifier, this can eliminate the effect of switching noise on output power signal. The block diagram of the designed excitation source is shown in Fig. 4.

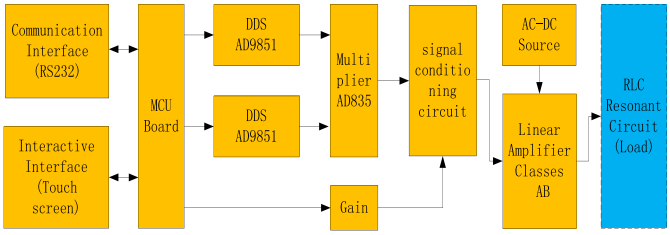

Fig. 4. Block diagram of the designed excitation source.

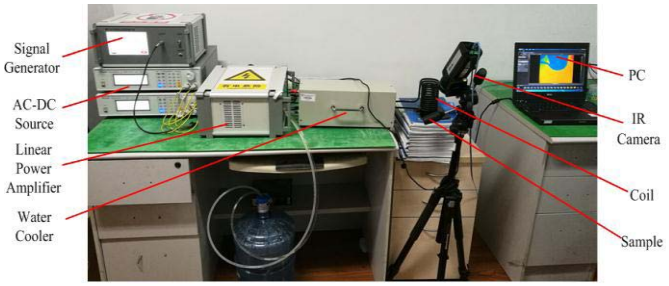

Fig. 5. Experiment setup.

Communication interface panel and configuration are interpreted as frequency tuning, control and phase modulation. These are loaded into the two DDS synthesizer AD9851 respectively by using the programmable MCU. A low frequency sinusoidal signal $u_1(t) = A_1 \cdot \sin(2\pi f_{lock}t)$ and a high frequency sinusoidal signal $u_2(t) = A_2 \cdot \sin(2\pi f_{ind}t)$ are generated as output of the two AD9851 and the inputs of the multiplier AD835, where A_1 and A_2 denote the amplitude. The output of the multiplier AD835 is $u_{o1}(t) = u_1(t) \cdot u_2(t)$ which is processed as filtering and gain adjusted through signal conditioning circuit to meet the impedance matching, input voltage range and bandwidth requirements of linear power amplifier. Thus, the output of the excitation source is $u_o(t) = k_1 \cdot k_2 \cdot u_{o1}(t)$ where k_1 and k_2 is the gain of signal conditioning circuit and linear power amplifier, respectively. Due to the load of the excitation source is a RLC series resonant circuit, the maximum current through L can be expressed as Eq.(12) when the resonance occurs.

$$\begin{aligned}i_{omax}(t) &= \frac{u_o(t)}{R}=\frac{A_1\cdot A_2\cdot k_1\cdot k_2}{R}\cdot u_{o1}(t)\\ &= I_m\cdot\sin\left(2\pi f_{lock}t\right)\cdot\sin\left(2\pi f_{ind}t\right)\end{aligned} \quad (12)$$

where R is the resistance of the RLC series resonant circuit, inductor L is the excitation coil, $i_{omax}(t)$ is the excitation current. Thus, adjusting the value of the output voltage u_o or R can vary the excitation current. Here, linear power amplifier is composed of two classes AB operational amplifier PA04 which are parallel connected to enlarge the maximum output current to 40A.

III. Experiment Setup

The experimental setup is shown in Fig. 5. The excitation source consists of AC-DC unit, signal generator and linear power amplifier who has a maximum power of 400W and 40A output current. The maximum excitation frequency is

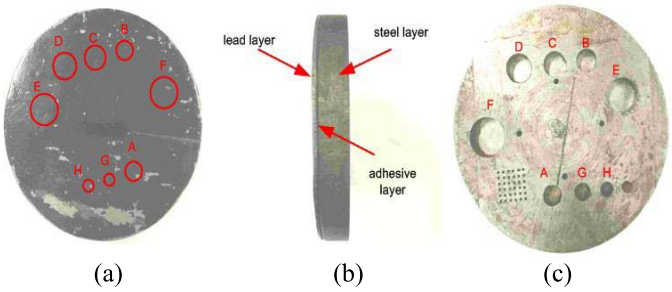

Fig. 6. Test sample. (a) Top. (b) Side. (c) Bottom.

250 kHz and can be adjusted according to the RLC resonant frequency. The range of the lock-in frequency is 0.01-99 Hz with a resolution of 2.328×10^{-4} Hz which can be set by RS232 interface or touch screen. A spiral coil is constructed to stimulate eddy current. The coil is made of 6.35 mm high conductivity hollow copper tube which has a outer diameter 76 mm and 13 coil turns. The inductance of the coil is 4.7uH tested at 100 kHz. Water cooling of coil is implemented to counteract direct heating of the coil. The IR camera, FLIR A655sc has an uncooled micro-bolometer with a high resolution 640× 480 array and its spectral range is 7.5-14μm. This camera has a sensitivity of 30mK and a maximum frame rate of 200Hz. In this study, the frame rate is set as 12.5 Hz.

A lead-steel sample which is made of lead and steel bonded by industrial EP adhesive is prepared as shown in Fig. 6. The sample includes three layer: lead layer, adhesive layer and steel layer shown as (a). The thickness of lead layer, adhesive layer and steel layer is 1.0mm, 0.1 mm and 5.0mm, respectively. In order to simulate the debonding defects, several holes with different diameters are made in the steel layer as the artificial defects shown as (c). The defects as marked with A, B, C, D, E, F, G are located in the steel layer with diameter 7 mm, 8 mm, 9 mm, 10 mm, 12 mm and 14 mm, respectively.

IV. Results and Analysis

A. Sensitivity of Detectability

The debonding defect of the lead-steel structure is an insulation defect, which obstructs the heat transfer that leads to a hot area on the surface of the sample. Detectability sensitivity is defined as temperature contrast between the defect area and the non-defective area. This can be expressed as follows:

$$T_{sen} = T_{def} - T_{non} \tag{13}$$

where T_{sen} is the temperature contrast, T_{def} denotes the mean temperature of the defect area, and T_{non} denotes the mean temperature of the non-defective area. Fig.7 is a top view which shows the relative location of defective area and sound area. The lift-off distance between the spiral coil and sample is 1 mm. In order to identify the defect, two regions of the ILT magnitude images were selected. These are the defective area S_1 and the sound area S_2, S_1 is selected from the actual defect area as shown in the shaded shape and S_2 is selected near the defect area. The defective area S_1 and the sound S_2 have the same radius r = 1 mm and the same distance d = 2 mm to coil.

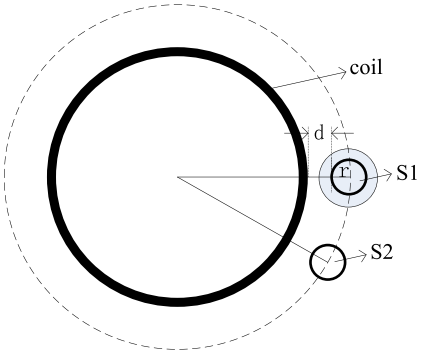

Fig. 7. The relative location of defective area and sound area.

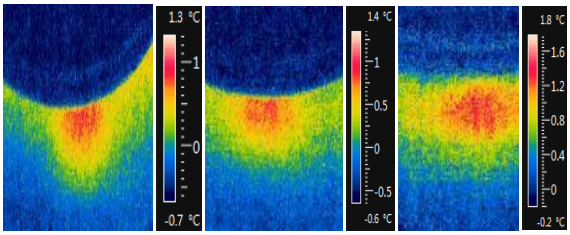

Fig. 8. Amplitude images with diameter of defects.

TABLE II
T_{sen} With Diameter of Defects

D/mm	14	12	10	9	8	7
Amplitudeof $T_{ac}(t)$ /°C	1.05	0.82	0.71	0.64	0.45	0.43
T_{sen}/°C	0.61	0.42	0.28	0.22	0.15	0.12

In Fig.3, the surface temperature $T_{sur}(t)$ consists of dc temporal component $T_{dc}(t)$ and ac oscillation components $T_{ac}(t)$.

$$T_{sur}(t) = T_{dc}(t) + T_{ac}(t) \tag{14}$$

$T_{dc}(t)$ can be obtained by polynomial fitting of variable time t based on Least-square method and ac oscillation components $T_{ac}(t)$ is thermal wave signal that can be obtained by subtracting dc temporal component $T_{dc}(t)$ [28]. Fig. 8 shows ILT amplitude images of detected defects with different size in lead-steel sample at lock-in frequency of 0.08 Hz. It can be seen that the maximum amplitude of *ac* oscillation component of the temperature is from 0.43° to 1.05° and detectability sensitivity T_{sen} is from 0.12° to 0.61° as shown in Table II. As expected, larger defects leads to higher temperature contrast. It indicates that the lager of the defect size, greater obstacle to the heat transfer is. The detectability sensitivity changes almost linearly with the defect diameter as shown in Fig.9.

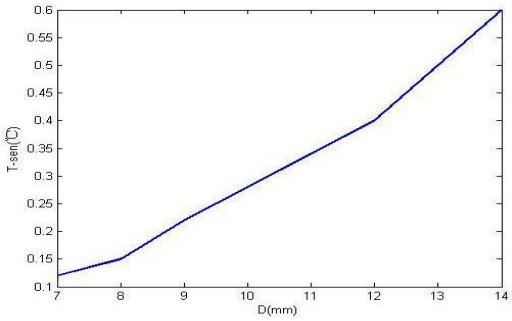

Fig. 9. Detectability sensitivity curves vs. diameter of defects.

B. Detectability of Amplitude and Phase Image Under Different Lock-in Frequency

Fig.10 shows the magnitude and phase images under different lock-in frequency where induction frequency is 47.5 kHz. For (a) to (j), the right panel is magnitude image and the left one is the phase image. It can be seen that the choice of lock-in frequency has a direct effect on the results of defect detection. The lock-in frequency should not be set too small. This can be shown in Fig.10 (a) while the defect could not be detected obviously in both magnitude and phase image under $f_{lock} =$ 0.024Hz. With the lock in frequency increases, the defect can be detected in the magnitude image as $f_{lock} = 0.049$Hz, this is shown in Fig.10 (b). As the lock frequency continues to increase, defect information is becoming progressively conspicuous in the phase image yet the magnitude information is becoming blurrer and less visible. These are shown from Fig.10 (c) to (i). However, the lock-in frequency should not be chosen too high as detectable sensitivity becomes poor when induction frequency $f_{lock} = 1.04$Hz as shown in Fig.10(j). The skin depth of lead and steel is 1.05 mm and 0.1 mm, respectively under $f_{ind} = 47.5\ kHz$. Thus, for the lead part, the induction thermography leads to volume heating and for the steel part it receives as surface heating. Since the defect is located near the spiral coil, the heat mechanism contains both transversely and longitudinally transmission.

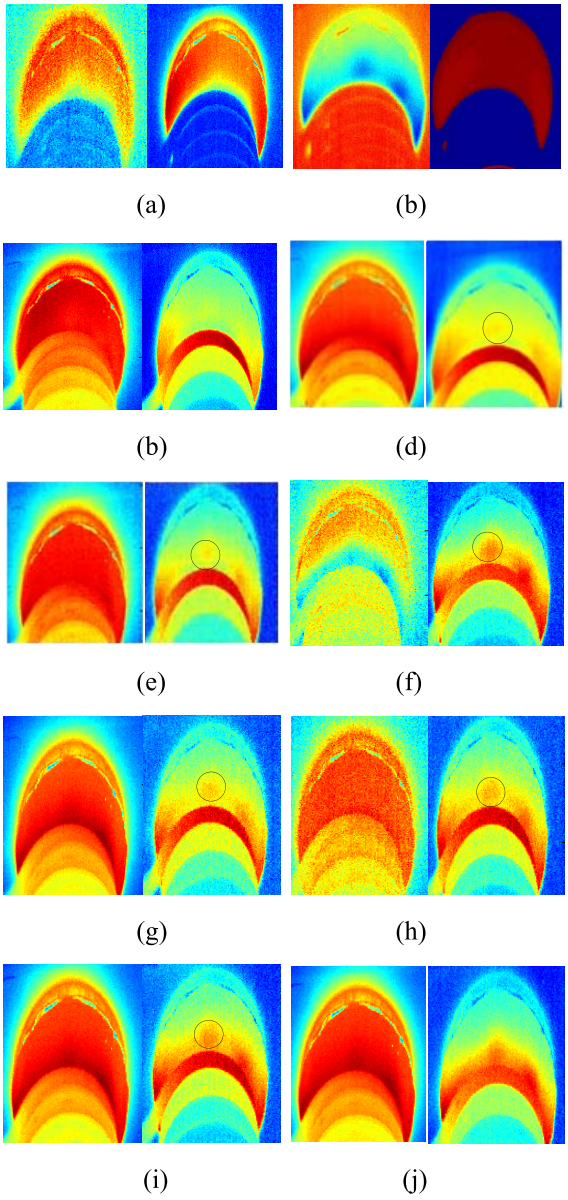

Fig. 10. Magnitude and phase images with lock-in frequency. (a) 0.024Hz. (b) 0.049Hz. (c) 0.058Hz. (d) 0.104Hz. (e) 0.208Hz. (f) 0.312Hz. (g) 0.416Hz. (h) 0.520Hz. (i) 0.728Hz. (j) 1.04Hz.

C. Comparison of ILT and ECPT

As discussed in the methodology session, ECPT records the temperature distribution of heating and cooling phases and adopts transient processing method to extract the maximum value, peak time and other characteristics methods to detect the defects of the material. To generate enough Joule heat within a short heating time, the excitation current is usually set large. Contrary with ECPT, in ILT system, the heating time usually includes several lock-in period that makes it require smaller excitation current because of the total energy required has been averaged in the longer heating time. If the excitation current is too small, the change of the temperature will linearly increase slower that leads to false alarm of detection. However, if the excitation current is too large, the strong electromagnetic field or thermal field can deteriorate the properties of the sample or make even more damage on the sample. As shown in Fig.11, the sample was damaged when an excitation current reaches 200A and maintains 500ms by using ECPT. It was directly damaged and the lead layer was burned by the strong electromagnetic and thermal field. Thus, in this study ILT is more suitable than ECPT.

D. Comparison of ILT and Optical Lock-in Thermography

Emissivity is a surface property of the investigated material which represents the ability to emit energy. It has a decisive impact on the interpretation of the thermal images. A surface with a low emissivity condition acts as a mirror that often makes the failed detection. Generally, using high emittance black paints on the investigated surface can solve this problem. However, it is not allowed in many situations. A sample without paints and with uneven emissivity is shown as Figure.12 (a). The test is investigated by using ILT and

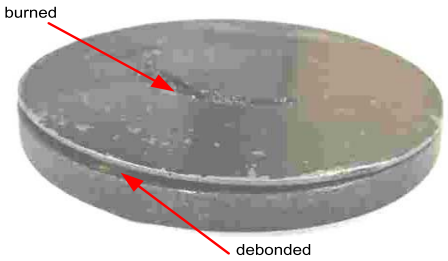

Fig. 11. Damaged sample.

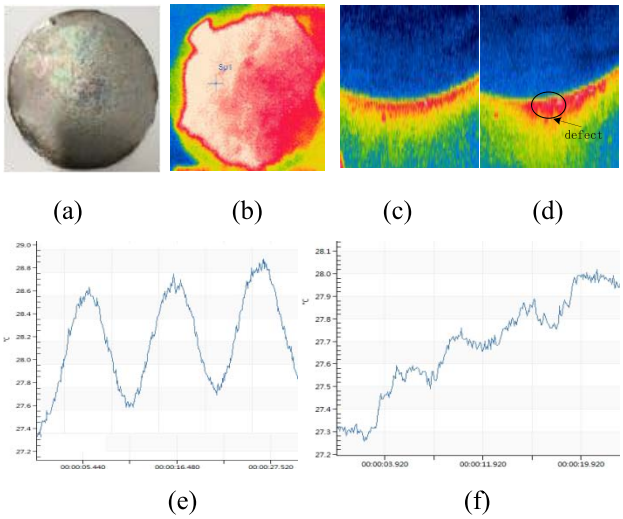

Fig. 12. Magnitude images and temperature evolution in ILT and OLT: (a) unpainted sample; (b) OLT result; (c) sound area in ILT; (d) defect area in ILT; (e) temperature evolution in ILT; and (f) the temperature evolution in OLT.

optical lock-in Thermography (OLT) techniques, respectively where two parallel 1kW halogen lamps is used in OLT. It can be seen that the defects cannot be detected in OLT and thermal image is blurred as shown in Figure.12 (b). The temperature evolution of one point on thermal image of the OLT is shown in Figure.12 (f). It is deteriorated heavily which only retains distorted lock-in characteristics. Conversely, as shown in Figure.12 (c), (d) and (e), the defect could be still detected despite of impaction of the low and uneven emissivity.

V. Conclusion and Future

The ILT technology has been proposed for the debonding defects detection of the lead-steel bonded material. Theoretical analysis of inductive lock-in thermography and the design of excitation source are introduced. The experiments have been conducted to demonstrate the feasibility detectability by using ILT. Experiments indicate that the detectability sensitivity of the defect changes almost linearly with the increase of the defect diameter and the selection of lock-in frequency has a direct effect on the detection performance. For the specific sample, the lock-in frequency should be selected empirically. In addition, the comparison and discussion of ILT with ECPT as well as OLT technique have been specified. Future work will investigates the optimization of the coil, detection of various geometry of multi-layers samples, advanced signal processing algorithms and quantitative analysis.

References

[1] A. Baldan, "Adhesively-bonded joints and repairs in metallic alloys, polymers and composite materials: Adhesives, adhesion theories and surface pretreatment," *J. Mater. Sci.*, vol. 39, no. 1, pp. 1–49, Jan. 2004.
[2] R. D. Adams and B. W. Drinkwater, "Nondestructive testing of adhesively-bonded joints," *NDT&E Int.*, vol. 30, no. 2, pp. 93–98, Apr. 1997.
[3] J. A. M. Ferreira, P. N. Reis, J. D. M. Costa, and M. O. W. Richardson, "Fatigue behaviour of composite adhesive lap joints," *Compos. Sci. Technol.*, vol. 62, no. 11, pp. 1373–1379, Aug. 2002.
[4] M. Quaresimin and M. Ricotta, "Life prediction of bonded joints in composite materials," *Int. J. Fatigue*, vol. 28, no. 10, pp. 1166–1176, Oct. 2006.
[5] H. K. Bui, G. Wasselynck, D. Trichet, and G. Berthiau, "Performance assessment of induction thermography technique applied to carbon-fiber-reinforced polymer material," *IEEE Trans. Magn.*, vol. 51, no. 3, Apr. 2015, Art. no. 8001804.
[6] C. Maierhofer, P. Myrach, M. Reischel, H. Steinfurth, M. Röllig, and M. Kunert, "Characterizing damage in CFRP structures using flash thermographyin reflection and transmission configurations," *Compos. B, Eng.*, vol. 57, pp. 35–46, Feb. 2014.
[7] J. Rantala, D. Wu, and G. Busse, "Amplitude-modulated lock-in vibrothermography for NDE of polymers and composites," *Nondestruct. Eval.*, vol. 7, no. 4, pp. 215–228, Apr. 1996.
[8] T. Zweschper, A. Dillenz, G. Riegert, D. Scherling, and G. Busse, "Ultrasound excited thermography using frequency modulated elastic waves," *Insight-Non-Destruct. Test. Condition Monitor.*, vol. 45, no. 3, pp. 178–182, Mar. 2003.
[9] E. Dehghani, F. Daneshjoo, A. A. Aghakouchak, and N. Khaji, "A new bond-slip model for adhesive in CFRP–steel composite systems," *Eng. Struct.*, vol. 34, pp. 447–454, Jan. 2012.
[10] X.-L. Zhao and L. Zhang, "State-of-the-art review on FRP strengthened steel structures," *Eng. Struct.*, vol. 29, no. 8, pp. 1808–1823, Aug. 2007.
[11] V. Dattoma, R. Marcuccio, C. Pappalettere, and G. M. Smith, "Thermographic investigation of sandwich structure made of composite material," *NDT&E Int.*, vol. 34, no. 8, pp. 515–520, Dec. 2001.
[12] C. Ibarra-Castanedo *et al.*, "Comparative study of active thermography techniques for the nondestructive evaluation of honeycomb structures," *Res. Nondestruct. Eval.*, vol. 20, no. 1, pp. 1–31, 2009.
[13] M. He and W. A. Hu, "A study on composite honeycomb sandwich panel structure," *Mater. Des.*, vol. 29, no. 3, pp. 709–713, 2008.
[14] R. Usamentiaga, P. Venegas, J. Guerediaga, L. Vega, and I. López, "Non-destructive inspection of drilled holes in reinforced honeycomb sandwichpanels using active thermography," *Infr. Phys. Technol.*, vol. 55, no. 6, pp. 491–498, Nov. 2012.
[15] S. Bagavathiappan, B. B. Lahiri, T. Saravanan, J. Philip, and T. Jayakumar, "Infrared thermography for condition monitoring—A review," *Infr. Phys. Technol.*, vol. 60, pp. 35–55, Sep. 2013.
[16] K. Chatterjee, S. Tuli, S. G. Pickering, and D. P. Almond, "A comparison of the pulsed, lock-in and frequency modulated thermography nondestructive evaluation techniques," *NDT&E Int.*, vol. 44, no. 7, pp. 655–667, Nov. 2011.
[17] G. Riegert, T. Zweschper, and G. Busse, "Lockin thermography with eddy current excitation," *Quant. Infr. Thermogr.*, vol. 1, no. 1, pp. 21–31, 2004.
[18] G. Riegert, A. Gleiter, and G. Busse, "Potential and limitations of eddy current lockin-thermography," *Proc. SPIE*, vol. 6205, pp. 62051E-1–62051E-8, Apr. 2006.
[19] J. Bohm and K.-J. Wolter, "Inductive excited lock-in thermography for electronic packages and modules," in *Proc. Int. Spring Seminar Electron. Technol.*, May 2010, pp. 190–195.
[20] B. Gao, W. L. Woo, and G. Y. Tian, "Electromagnetic thermography nondestructive evaluation: Physics-based modeling and pattern mining," *Sci. Rep.*, vol. 6, May 2016, Art. no. 25480.
[21] P. Silvester and R. L. Ferrari, *Finite Elements for Electrical Engineers*, 3rd ed. Cambridge, U.K.: Cambridge Univ. Press, 1996.
[22] B. Gao, W. L. Woo, Y. He, and G. Y. Tian, "Unsupervised sparse pattern diagnostic of defects with inductive thermography imaging system," *IEEE Trans. Ind. Informat.*, vol. 12, no. 1, pp. 371–383, Feb. 2016.
[23] J. Wilson, G. Y. Tian, I. Z. Abidin, S. Yang, and D. Almond, "Modelling and evaluation of eddy current stimulated thermography," *Nondestruct. Test. Eval.*, vol. 25, no. 3, pp. 205–218, 2010.

[24] B. Gao, Y. He, W. L. Woo, G. Y. Tian, J. Liu, and Y. Hu, "Multidimensional tensor-based inductive thermography with multiple physical fields for offshore wind turbine gear inspection," *IEEE Trans. Ind. Electron.*, vol. 63, no. 10, pp. 6305–6315, Oct. 2016.
[25] G. Busse and A. Rosencwaig, "Subsurface imaging with photoacoustics," *Appl. Phys. Lett.*, vol. 36, no. 10, pp. 815–816, 1980.
[26] R. L. Thomas, J. J. Pouch, Y. H. Wong, L. D. Favro, P. K. Kuo, and A. Rosencwaig, "Subsurface flaw detection in metals by photoacoustic microscopya," *J. Appl. Phys.*, vol. 51, no. 2, pp. 1152–1156, 1980.
[27] X. P. Maldague and S. Marinetti, "Pulse phase infrared thermography," *J. Appl. Phys.*, vol. 79, no. 5, pp. 2694–2698, 1996.
[28] J. Liu, Y. Liu, F. Wang, and Y. Wang, "Study on probability of detection (POD) determination using lock-in thermography for nondestructive inspection (NDI) of CFRP composite materials," *Infr. Phys. Technol.*, vol. 71, no. 2, pp. 448–456, 2015.

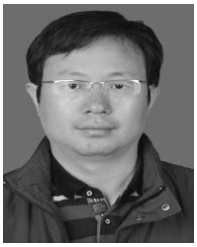

Yuyu Zhu received the B.S. degree in automation from the Southwest University of Science and Technology, China, in 2002, and the M.Sc. degree in control theory and control engineering from the Southwest University of Science and Technology, in 2009. He is currently pursuing the Ph.D. degree with the University of Electronic Science and Technology of China. He is an Associate Professor with the School on Monitoring and Control Technology and Power Electronics Technology. His research interests include nondestructive testing and evaluation, power electronics technology. He has developed several equipment and coordinated several research projects.

Bin Gao (M'12–SM'14) received the B.Sc. degree in communications and signal processing from Southwest Jiao Tong University, China, in 2005, the M.Sc. (With Distinction) degree in communications and signal processing, and the Ph.D. degree from Newcastle University, U.K., in 2011. He was a Research Associate with Newcastle University working on wearable acoustic sensor technology. He is currently a Professor with the School of Automation Engineering, University of Electronic Science and Technology of China, Chengdu, China. His research interests include sensor signal processing, machine learning, social signal processing, nondestructive testing and evaluation where he actively publishes in these areas. He is a very active reviewer for many international journals and long standing conferences. He has coordinated several research projects from the National Natural Science Foundation of China.

Gui Yun Tian (M'01–SM'03) received the B.Sc. degree in metrology and instrumentation and the M.Sc. degree in precision engineering from the University of Sichuan, Chengdu, China, in 1985 and 1988, respectively, and the Ph.D. degree from the University of Derby, Derby, U.K., in 1998. From 2000 to 2006, he was a Lecturer, a Senior Lecturer, a Reader, a Professor, and Head of the Systems Engineering Group, respectively, with the University of Huddersfield, U.K. Since 2007, he has been based at Newcastle University, Newcastle upon Tyne, U.K., where he has been the Chair Professor of Sensor Technologies. He is currently an Adjunct Professor with the School of Automation Engineering, University of Electronic Science and Technology of China. He has coordinated several research projects from the Engineering and Physical Sciences Research Council, the Royal Academy of Engineering and FP7, on top of this he also has good collaboration with leading industrial companies such as Airbus, Rolls Royce, BP, nPower, Networkrail, and TWI among others.

Wai Lok Woo was born in Malaysia. He received the B.Eng. (First Class Hons.) degree in electrical and electronics engineering and the Ph.D. degree from the Newcastle University, U.K. He is currently a Senior Lecturer and the Director of Operations with the School of Electrical and Electronic Engineering. He has published over 250 papers on these topics in various journals and international conference proceedings. His major research is in the mathematical theory and algorithms for nonlinear signal and image processing. This includes areas of machine learning for signal processing, blind source separation, multidimensional signal processing, signal/image deconvolution, and restoration. He has an extensive portfolio of relevant research supported by a variety of funding agencies. He received the IEEE Prize and the British Scholarship to continue his research work. He is currently an associate editor of several international journals. He has served as a lead-editor of journals' special issues.

Guangping Tang received the B.Sc. degree in material science and engineer from Zhejiang University, Hangzhou, China, in 1991, and the M.Sc. degree in mechanical engineer from Sichuan University, Chengdu, China, in 2003. Since 1991, he has been a Researcher with the China Academy of Engineer Physics, Mianyang, China. His research interests include engineer materials, functional materials, surface modification with laser, and their properties evaluation.

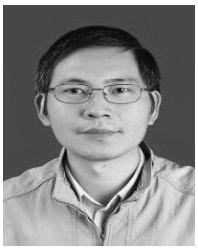

Chaoming Sun received the M.Sc. degree from the School of Mechatronic Engineering and Automation, Shanghai University, China, in 2002. He is currently a Senior Engineer with the Institute of Machinery Manufacturing Technology, China Academy of Engineering Physics, Mianyang, China.

Jianwen Li received the M.Sc. degree from the School of Materials Science Professionals, Sichuan University, China, in 2001. He is currently a Senior Engineer with the Institute of Machinery Manufacturing Technology, China Academy of Engineering Physics, Mianyang, China. His research interests include nondestructive testing technologies of matel materials.